A FRACTURE MECHANICS CONTRIBUTION TO FUEL ELEMENT DESIGN AND ANALYSIS*

P.S. CHOPRA, T.S. WU and G.L. HOFMAN

EBR-II Project, Argonne National Laboratory, Argonne, Illinois 60439, U.S.A.

SUMMARY

This paper demonstrates the usefulness of a finite element fracture mechanics technique for evaluating the structural integrity of fast breeder reactor fuel element cladding. In an earlier work, Chopra (SMiRT-2 Paper C 2/5*) presented a technique for analyzing the creep rupture of fuel element cladding based upon linear elastic finite element solutions for strain energy release rates and stress intensity factors. Finite element solutions are now obtained which include the influence of material non-linearity due to creep and plastic deformation.

Cladding failures in EBR-II Mark II driver fuel elements are evaluated with the fracture mechanics technique. Crack growth rates are obtained from destructive examinations of a series of fuel element cladding at varying burnups. These are related to normalized stress intensity factors to obtain the effective creep fracture toughness of the irradiated cladding.

The accuracy of the fracture mechanics solutions for fuel element cladding studies depends upon the ability to determine the nominal stress in the cladding due to the simultaneous action of internal gas pressure and pressure due to expanding fuel. Such nominal stresses may be obtained from one-dimensional axisymmetric fuel element performance codes and used as input for the two-dimensional finite element solutions. Alternatively, as is done in the present study, a lower bound for the nominal stresses may be obtained by the use of internal gas pressure (which is strictly correct for the plenum region) and an upper bound can be obtained by incrementing the internal pressure by an amount equal to the out-of-pile fuel compressibility.

The influences of multiple secondary fractures on the inner surface of the fuel element cladding and non-axisymmetric loadings such as those resulting from fuel particle wedging are accounted for readily by the finite element fracture mechanics technique. The technique provides fast breeder reactor fuel element designers and analysts with an alternative basis for selecting cladding materials and for comparing various fuel element designs.

* This work has been performed under the auspices of the United States Atomic Energy Commission.

1. Background

The prediction of cladding failure in fast reactor fuel elements is complicated by the simultaneous occurrence of low cycle fatigue and creep at elevated temperature in the presence of radiation and a corrosive environment. A step toward such failure prediction is to evaluate the influence of local defects in the cladding on its creep rupture behavior under service loads. Cladding defects may be inherent or may result internally from fission-product attack or externally from sodium corrosion and mechanical wear. Service loads include internal pressure due to fission gas and fuel swelling and local loads caused by fuel cracking which may sometimes lead to wedging of a fuel particle between the fuel pellet and the cladding. Interaction loads also may exist between the cladding and the spacer wire, between the fuel element and the surrounding elements, and between the element cluster and the subassembly duct.

Other investigations of cladding failure have assumed axisymmetric loads in a one-dimensional model and have treated defects by assuming only reduction of the cladding thickness by the depth of the defect. In a previous investigation Chopra [1] showed that such axisymmetric treatment overestimates the strength of the cladding by ignoring the stress concentrations near the tip of a defect or crack. To account for these defects, a finite element fracture mechanics technique was proposed. In this presentation, the finite element technique is extended to compute fracture parameters from elastic analyses, for fuel element claddings of differing geometries. Preliminary results of creep analyses also are presented along with values of modified fracture parameters. The influence of local loads, to simulate in a simple manner the effect of fuel particle wedging, on cladding fracture is also investigated.

2. Analysis Approach

In reference [1] a simple relationship was proposed between defect size and location, nominal clad hoop stress or internal pressure, time to rupture, and the corrosive activity of the surrounding media in the form:

$$\sigma = \{K_{ec}(a/h,t_r,q)\}/\{\pi^{1/2}a^{1/2}F(a/h)\} \tag{1}$$

where σ is the nominal hoop stress, a is the initial depth of a longitudinal crack, h is the cladding thickness, t_r is the time to rupture, and q is a structure sensitive parameter which accounts for the influence of the environment. F(a/h) is a function, obtained from finite element solutions, which accounts for the geometric differences between the present structure and the classical Griffith plate. The function $K_{ec}(a/h,t_r,q)$ can be obtained from creep rupture tests of cladding with varying initial flaw depths and times to rupture under corrosive as well as inert environments.

$$F(a/h) = \{G_T E/[(1-\nu^2)\pi a\sigma^2]\}^{1/2} \tag{2}$$

where E is Young's modulus, ν Poisson's ratio. The total strain energy release rate G_T is evaluated by direct calculation of total energies associated with finite element solutions of sequential boundary value problems.

3. Description of Finite Element Investigations

Three types of fuel element claddings were investigated: the AISI Type 316 stainless steel on experimental mixed-oxide fuel elements in the EBR-II [1], the AISI Type 304 stainless steel on driver elements in EBR-II [2] and the Type 1.4981 stainless steel used in the German experimental program [3]. The cladding geometries are shown in Fig. 1.

Elastic solutions for the Type 316 cladding with internal and external longitudinal flaws were reported earlier [1]. Some creep analysis results on this type of cladding are presented here and compared with previous results. Elastic solutions are obtained for the Type 304 cladding with external longitudinal flaws under internal pressure, and with internal flaws under internal pressure as well as a local load. Elastic solutions are also obtained for the Type 1.4981 cladding with external longitudinal flaws under internal pressure.

The elastic analyses were conducted with the code derived by Wilson [4] and the creep analyses with CREEP-PLAST code developed by Rashid [5]. Both finite element codes were modified to compute the strain energy stored in the cladding. The elastic code was modified with the exact energy expression given in reference [1]. The CREEP-PLAST code was modified to compute an approximate energy expression in terms of the integral of the product of the equivalent stress and strain in each element of the structure. This approximation was selected for preliminary studies in view of its simplicity compared to the more rigourous expression given in reference [1]. The approximation yields an energy rate parameter, P, given by:

$$P = \frac{\Delta \int \sigma^* \varepsilon^* dv}{\Delta a_T} \qquad (3)$$

where σ^* and ε^* are the equivalent stresses and strains obtained from the Von Mises yield surface.

In each type of cladding, a pair of opposed longitudinal flaws were assumed to exist on either the inner or the outer surface of the cladding. Such symmetry allowed one quarter of the cladding only to be modeled. The assumption that the flaws are long compared to the cladding diameter, justified the use of plane strain conditions.

The finite element mesh employed in the elastic analyses was divided into thirty-two equal divisions radially in the neighborhood of the crack as shown in Fig. 1. In previous analyses of the Type 316 cladding twenty-four divisions were used across the cladding thickness. The mesh used for the creep analysis had forty-eight triangular elements across its thickness in the neighborhood of the crack.

4. Elastic Analyses

Selected elastic solutions for the three claddings are presented in Figs. 2-5. Figure 2 shows the maximum stress in the element immediately ahead of the tip of an external crack as a function of the relative crack depth, a/h. The ratio of the outer diameter of the cladding to the inner diameter, $w = R_2/R_1$, and the inner diameter to the cladding thickness, R_1/h, are also shown. As expected, stresses are higher for larger crack depths and increase faster with increasing crack depths. The stresses also are highest for the cladding with the smallest diameter ratio w, and the highest ratio of R_1/h for the same relative crack depth (a/h). The same trends are observed in Fig. 3 for the normalized stress intensity factor as a function of a/h.

Figure 4 shows the variation of the total strain energy release rate, G_T, with a/h, which follows the pattern observed in the two previous figures. The thicker Type 1.4981 and Type 316 claddings have a deeper crack than the Type 304 cladding for the same value of a/h, and the curves for the former cladding types are very close. However, the results for the Type 316 cladding were obtained using a slightly coarser finite element mesh [1] and since the present method provides a lower bound solution for G_T for primary crack propagation [6], refinement of the mesh for the Type 316 cladding studies would provide higher values of G_T. The results of Figs. 2 through 4 are in general agreement with those presented by Shannon [7] for thick-walled cylinders with diameter ratios greater than 1.5.

The normalized stress intensity factor, F(a/h), is shown in Fig. 5 as a function of the relative crack depth. As earlier, the results suggest that for a given ratio of a/h, the geometry of the Type 316 cladding provides a higher value of F(a/h).

Figure 6 shows the results of simulating an internal crack under uniform internal pressure and a local load. This analysis was conducted to simulate the possible effect of loads from a fuel particle wedged between the fuel pellet and the cladding. Curve A corresponds to an internal crack in the Type 304 SS cladding subjected to fluid pressure. Curves B and C show the values of F(a/h) when a local pressure of 2000 psi and 4000 psi, respectively, is applied adjacent to the crack, as shown in the figure. The results indicate that F(a/h) decreases as the local load is increased. That is, the local load tends to prevent the propagation of the specified crack. The value of F(a/h) increases significantly however when the point of application of the local load is moved from the crack by an angle of 15° as shown by curve D. The results of Fig. 6 demonstrate that crack propagation, measured in terms of F(a/h), is sensitive to the relative locations of the crack and local loads.

5. Creep Analysis

Preliminary results obtained using the CREEP-PLAST program [6] and the creep equation for Type 316 stainless steel proposed by Straalsund [8] are shown in Figs. 7 to 11.

Figure 7 shows how the stresses and strains vary in an element just ahead of the tip of an internal crack, when the cladding is subjected to the pressure history shown. In the time interval $0<t<1000$ hr. the strain ϵ_x, increases monotonically while the strain, ϵ_y, decreases monotonically. Both ϵ_x and ϵ_y flatten off at $t = 800$ hr. No significant effects are observed after $t = 1000$ hr. except for the anticipated dip in ϵ_x and ϵ_y corresponding to the dip in the pressure. The increase in σ_x within 400 hr$<t<1000$ hr. may be explained by the change with time of stress distribution across the cladding wall, as shown in Fig. 8. Stresses in the inner elements increase with time while those in the outer elements decrease. This stress redistribution, while the cladding deforms, depends upon the creep law prevailing.

Figure 9 shows the energy rate parameter, P, as a function of crack depth for times up to 500 hrs. The curves resemble those obtained for strain energy release rates G_T in the elastic case. As suggested previously [1] creep deformation causes time-dependent changes in energy release rates. The parameter P, increases with time up to approximately 200 hrs. and then decreases. This is illustrated more clearly in Fig. 10. This figure shows the modified normalized stress intensity factors, $\bar{F}(a/h,t_r)$ obtained from eq. (2) by replacing G by P.

The results shown in Fig. 10 were used to compute a modified fracture toughness parameter, $\bar{K}_{ec}$ from creep rupture tests [9]. The specific value of $\bar{F}(a/h,t_r)$ was used which corresponded to the time to rupture for the cladding. This preliminary application is shown in Fig. 11. Also shown are the values of K_{ec} that were obtained previously using elastic solutions for F(a/h). The spread between the fracture toughness curves is reduced in the present creep application. This result is consistent with a previous suggestion [1] that a uniform value of fracture toughness would be obtained if all effects of material and geometric non-linearity could be accounted for in computing the normalized stress intensity factors.

6. Application to Type 304 SS Cladding

The EBR-II Mark II driver fuel element consists of a uranium alloy fuel pin that is sodium bonded to an annealed Type 304L stainless steel cladding [2]. Such elements have been irradiated to cladding failure in sodium filled secondary capsules. Five elements that have exhibited cladding failures originating from the outer surface. A typical fracture is illustrated in Fig. 12 by a series of transverse sections taken from the axial fracture tip to the center of the fracture. Scanning Electron Microscopy of the fracture revealed the transition from a finely structured surface adjacent to the cladding interior to a coarse dimpled face towards the cladding exterior, which indicated that the cracks initiated at the outer surface. The growth of these external cracks was obtained by examining sibling unfailed elements that were withdrawn from the reactor at regular intervals. Metallography showed that a large number of cracks were present at the outer surface of all samples, and the depth of the cracks increased as irradiation progressed, as shown in Fig. 13. The actual maximum crack depth is expected to be larger than the maximum observed depth since the probability of sectioning the largest crack in a particular fuel element at its largest depth is less than one. Also shown in Fig. 13 is the observed cladding failure density distribution for the Mark II fuel elements analyzed here.

The accuracy of the application of fracture mechanics depends upon the ability to determine the nominal stress in the cladding due to the simultaneous action of internal gas pressure and pressure due to expanding fuel. Gas pressure was determined by sampling nonfailed fuel elements at various times [10]. The use of gas pressure alone provides a lower bound for the computed stress intensity factors. An upper bound solution can be obtained by adding a component of internal pressure equal to the out-of-pile fuel compressibility [2]. The stress history used in the present application is shown in Fig. 14. The stress is small up to about 2000 hours because neither significant gas release nor fuel-cladding contact takes place until then. Beyond 2000 hours, stress continually increases due to fission gas release from the fuel.

The time to cladding failure for various initial crack depths were obtained from Fig. 13. These data were then used with eq. (1) to solve for the effective creep fracture toughness, K_{ec}. The nominal stress σ, was obtained from Fig. 14 as the average stress during the service lifetime of the cladding. Results of this application are shown in Fig. 15. As expected, the toughness, K_{ec}, was found to be higher if the failed cladding had been exposed to both gas pressure and fuel loading, as shown by curve A. Curves A and B converge toward a failure time of 10,000 hrs. as the value of K_{ec} tends to zero. The true fracture toughness of the cladding is higher than that shown in Fig. 15, since the current creep fracture model ignores the fatigue damage experienced during normal reactor operations.

Also shown in Fig. 15 are the results obtained previously [1] for the effective creep fracture toughness of Type 316 cladding in a corrosive environment. The agreement between the results for short-term creep rupture tests and the current results for long-term service failures is coincidental and interesting.

The relationship between crack growth rates da/dt and the average elastic stress intensity factor also was investigated in the manner described earlier [1]. The results are shown in Fig. 16. As noted for Fig. 15, the growth rates for the Type 304 cladding are similar to those previously reported for the Type 316 cladding. The damaging effect of fatigue was again ignored in the case of the Type 304 cladding.

7. Conclusions

The elastic finite element fracture mechanics technique can be used to evaluate quantitatively the creep fracture resistance of fast breeder reactor fuel element cladding. The influence of defects and non-axisymmetric loading can be readily treated. Further work is required to develop the non-linear model which will provide a more accurate simulation of creep fracture kinetics. In the meantime, the elastic model can be used by designers and analysts to compare various fuel element designs under a wide range of loads that is limited only by the capability of the finite element code employed.

Acknowledgements

The authors appreciate the technical discussions held with Professor Dr. H. Kämpf of Hargesheim, Germany, and with Mr. J. D. B. Lambert of the EBR-II Project, Argonne National Laboratory, U.S.A.

References

[1] CHOPRA, P. S., "Finite Element Fracture Mechanics Analysis of Creep Rupture of Fuel Element Cladding," Nuclear Engineering and Design, Vol. 29, pp. 7-21, November 1974.

[2] WALTER, C. M., et al, "EBR-II Driver-Fuel Qualification and Performance," Nucl. Met., Vol. 19, pp. 182-202 (1973).

[3] DIETZ, W., Private Communication, September 1972.

[4] WILSON, E. L., "Structural Analysis of Axisymmetric Solids," AIAA J., Vol. 3, 1965.

[5] RASHID, Y. R., "Analysis of Two-Dimensional Problems under Simultaneous Creep and Plasticity," GEAP-10546, January 1972.

[6] CHOPRA, P. S., "Finite Element Simulation of Secondary Cracking during Brittle Fracture," Ph.D. Dissertation, University of Washington, Seattle, 1971.

[7] SHANNON, R. W. E., "Stress Intensity Factors for Thick-Walled Cylinders," Int. J. Pres. Ves. and Piping, Vol. 2, pp. 19-29 (1974).

[8] STRAALSUND, J. L., "Working Group Recommendations for Metal Swelling and Creep Equations for Use in LIFE, HEDL TC-68, March 1974.

[9] KING, R. T., et al, "Biaxial Creep Rupture Properties of Defective Stainless Steel Tubing," ORNL-TM-3711, Oak Ridge National Laboratory, April 1972.

[10] HOFMAN, G. L. and JOHNSON, D. L., "Semi Empirical Correlations for the Fission Gas Release from Fast Reactor Fuels," Trans. ANS Annual Meeting, June 1975.

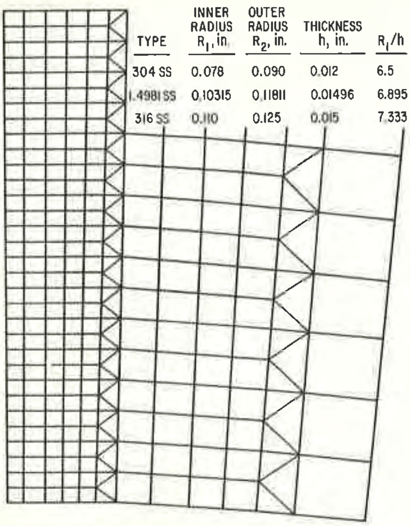

Fig. 1. Local Description of Finite Element Mesh Used for Elastic Analyses.

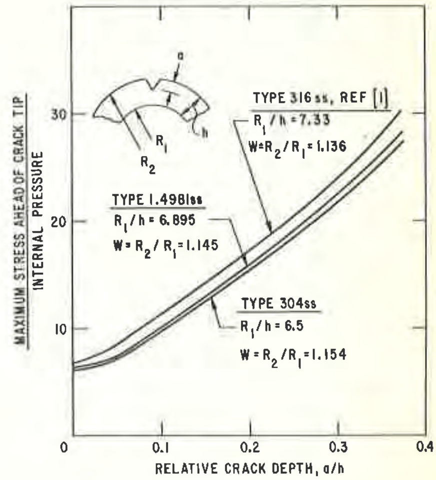

Fig. 2. Influence of External Crack Depth on the Maximum Elastic Stress in the Cladding.

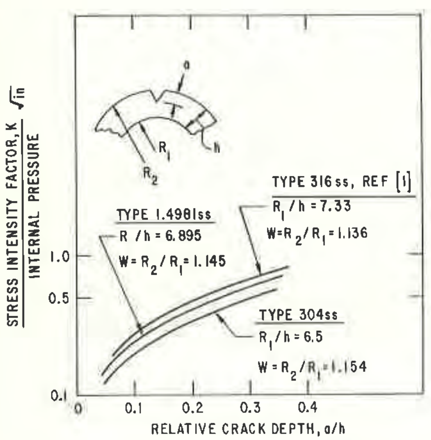

Fig. 3. Stress Intensity Factors, K, for External Cracks.

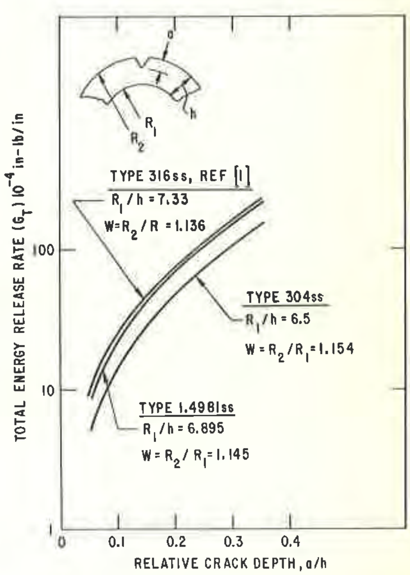

Fig. 4. Variation of Total Strain Energy Release Rates as a Function of Crack Depth.

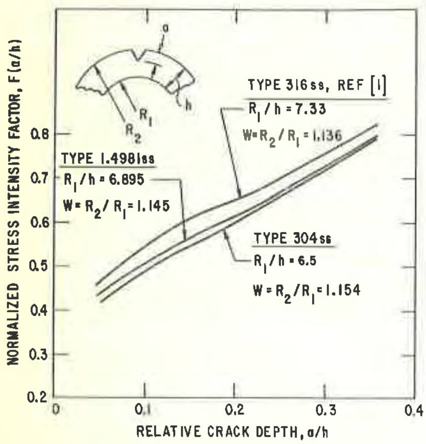

Fig. 5. Normalized Stress Intensity Factors, F, for External Cracks.

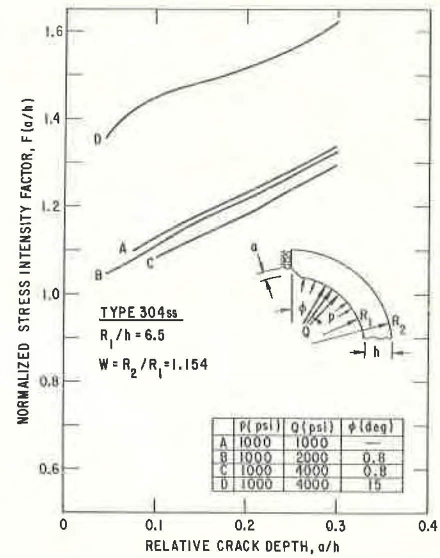

Fig. 6. Influence of Local Load on the Normalized Stress Intensity Factor, F, for Internal Cracks.

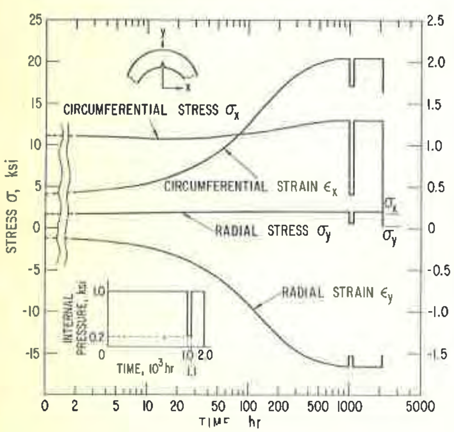

Fig. 7. Time Variation of Stresses and Strains in an Element just Ahead of the Tip of an Internal Crack.

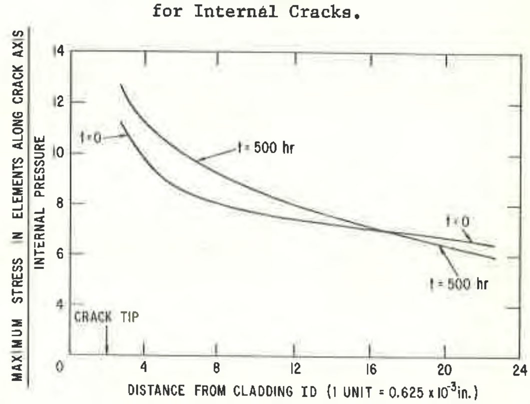

Fig. 8. Distribution of Maximum Stress Along Crack Axis.

C 4/1

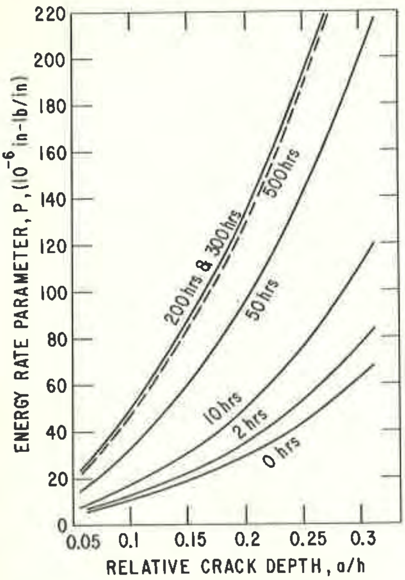

Fig. 9. Influence of Crack Depth on the Energy Rate Parameter, P, at Various Times.

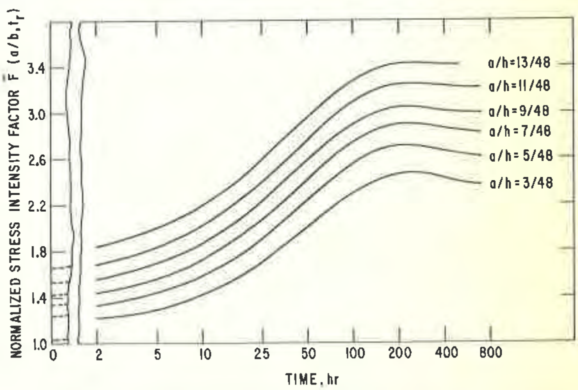

Fig. 10. Influence of Time on the Normalized Stress Intensity Factor, $\bar{F}$, for Various Crack Depths.

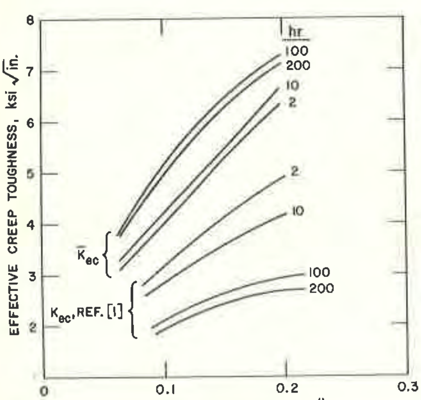

Fig. 11. Effective Creep Fracture Toughness, K_{ec} and $\bar{K}_{ec}$, as a Function of Crack Depth for Various Rupture Times.

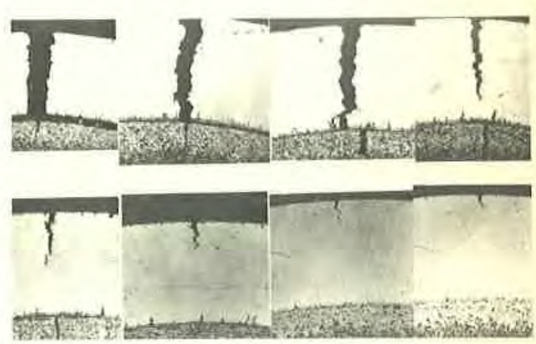

Fig. 12. Series of Transverse Sections Through an Axial Crack in an EBR-II Driver Fuel Cladding.

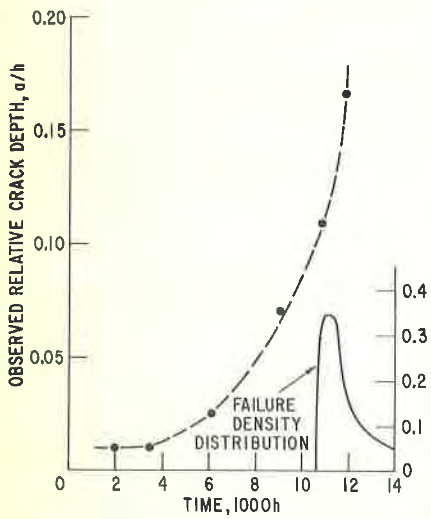

Fig. 13. Maximum Observed Crack Depth as a Function of Time at Power for EBR-II Driver Fuel Elements.

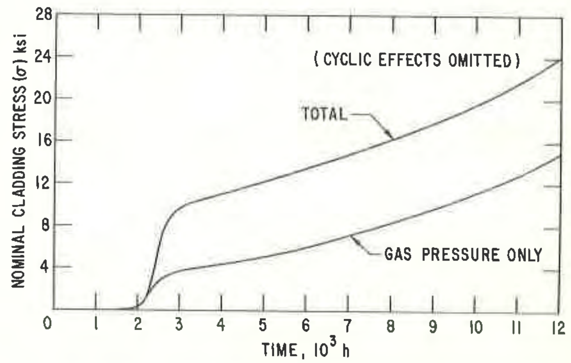

Fig. 14. Estimated Cladding Hoop Stress in EBR-II Driver Fuel Elements at Power as a Function of Time, Ref. [10].

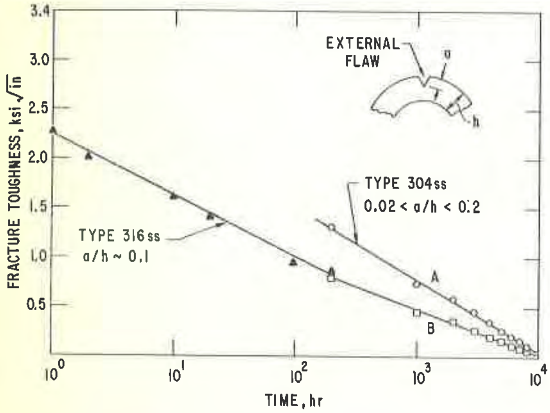

Fig. 15. Fracture Toughness of Types 304 and 316 Cladding as a Function of Rupture Time.

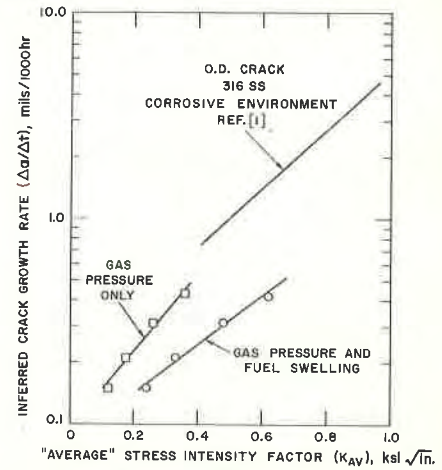

Fig. 16. Inferred Crack Growth Rates, $\Delta a/\Delta t$, for Types 304 and 316 Cladding as a Function of the Average Elastic Stress Intensity Factor K_{AV}.